Exploring potential quantum spin liquid state in a quasi-one-dimensional magnetic chain

Rahul Kumar [1], Kiwan Nam,[2] Seong-Hoon Kim,[2] Kee Hoon Kim,[2] and A. Sundaresan [1,*]

[1]*School of Advanced Materials, and Chemistry and Physics of Materials Unit, Jawaharlal Nehru Centre for Advanced Scientific Research, Bangalore-560064, India*

[2]*Department of Physics and Astronomy and Institute of Applied Physics, Seoul National University, Seoul 151-747, Republic of Korea*

(Received 18 October 2023; revised 21 May 2024; accepted 28 May 2024; published 27 June 2024)

This paper presents a comprehensive investigation of $NaYbTe_2O_7$ through a range of physical property measurements. A detailed examination of its crystal structure uncovers the formation of quasi-one-dimensional magnetic chains of Yb^{3+} ions along the b axis, with a substantial separation of approximately 6.3 Å between these chains. This unique arrangement of Yb ions positions $NaYbTe_2O_7$ as an ideal candidate for exploring one-dimensional magnetism. Magnetic measurements confirm the absence of a long-range magnetic ordering down to 0.4 K; however, they indicate the emergence of magnetic correlations below 1 K. The analysis of the inverse magnetic susceptibility corroborates that the ground state can be described as a Kramers doublet, indicating $J_{\text{eff}} = 1/2$. Our findings from magnetization measurements align with the results from temperature and magnetic field-dependent heat capacity measurements, both of which suggest robust magnetic correlations among Yb^{3+} ions. Moreover, heat capacity measurements reveal no long-range magnetic ordering down to 0.285 K. The assertion of these magnetic correlations is further reinforced by thermal conductivity measurements, which confirm the scattering of phonons due to magnetic excitations at low temperatures. Considering the combination of low dimensionality, $J_{\text{eff}} = 1/2$, the absence of magnetic ordering down to 0.285 K, and the presence of strong magnetic correlation below 1 K, we suggest that these results are indicative of a potential quantum spin liquid (QSL) state in $NaYbTe_2O_7$.

DOI: 10.1103/PhysRevB.109.224429

I. INTRODUCTION

Low dimensional quantum magnets offer a compelling platform for exploring systems governed by pronounced quantum and thermal fluctuations [1]. In particular, significant attention has been directed toward the one-dimensional (1D) J_1-J_2 quantum Heisenberg model, where an element of frustration is introduced through the parameter J_2. Theoretical investigations of such systems have indicated that the emergence of distinct quantum phases depends on factors like $\alpha = J_2/J_1$, applied magnetic fields, and axial exchange anisotropy [2–5]. This model has found experimental realization in a variety of compounds containing 3d elements, including but not limited to Li_2CuO_2 [6–8], $LiCuSbO_4$ [5], $SrCuO_2$ [9], $LiCuVO_4$ [10–12], Li_2CuZrO_4 [13], and $A_2Cu_2Mo_3O_{12}$ ($A = Rb$, Cs) [14,15]. Additionally, this model has been explored in a selected group of rare-earth-based compounds such as $YbAlO_3$ [16] and $TbScO_3$ [17]. However, the presence of large anisotropic orbital-dominated moments favors Ising or XXZ types of interactions rather than Heisenberg. Despite these assumptions, the Yb Kramers doublets exhibit distinct behavior from classical Ising spins. For example, the exchange processes among pseudospins ($J_{\text{eff}} = 1/2$) within the same chain involve quantum-origin spin flip terms, challenging the notion of their classical behavior [16,18]. The investigation on rare earth compounds has unveiled unconventional quantum phases and the presence of substantial anisotropic orbital-dominated moments, which can lead to fractional quantum excitations [18].

The strong spin-orbit coupling (SOC) combined with localized electrons in the $4f$ orbitals of rare earth elements makes these materials prime candidates for exploring strongly correlated physics. In systems characterized by an odd number of $4f$ electrons, the intricate interplay between the crystalline electric field and SOC assumes a central role in resolving degeneracy, ultimately leading to the formation of Kramers doublet states. This phenomenon holds significant promise for understanding and harnessing the unique electronic and magnetic behaviors exhibited by these materials. The rare earth compounds containing Yb are of particular interest as they have garnered significant attention in the pursuit of realizing QSLs owing to their $J_{\text{eff}} = 1/2$ Kramers doublet ground state [19–21]. The low-dimensional arrangement of Yb ions, e.g., 1-D chain, triangular lattice, and kagome lattice, intertwined with the intricate interplay of competing exchange interactions, set the ideal backdrop for the emergence of the quantum spin liquid phenomenon. Recent developments have highlighted several Yb-based compounds, such as $YbMgGaO_4$ [22], $NaYbO_2$ [20], and $Ba_3Yb_2Zn_5O_{11}$ [21], as potential candidates for hosting quantum spin liquid behavior within triangular or pyrochlore magnetic lattices. In this context, we embark on a journey to address the fundamental question of uncovering a QSL state within a compound characterized by a quasi-one-dimensional lattice.

*Contact author: sundaresan@jncasr.ac.in

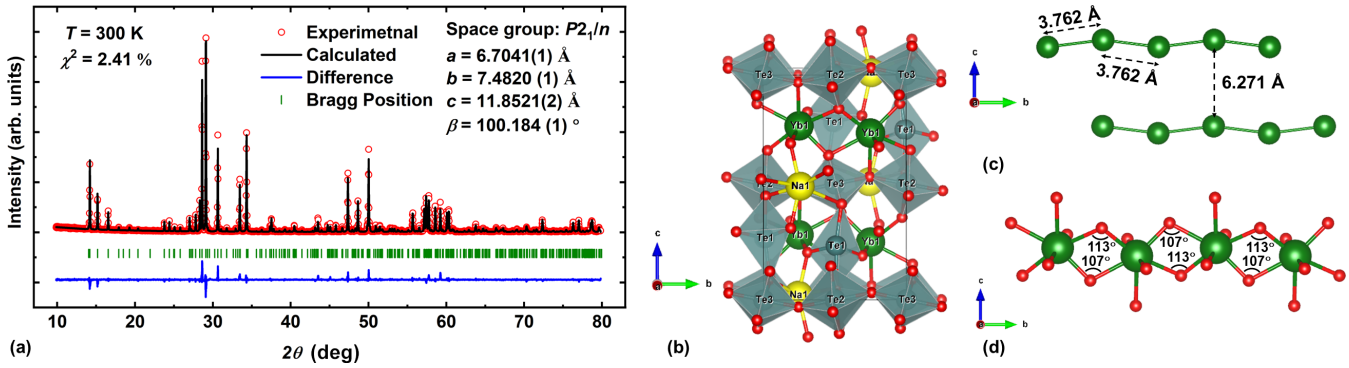

FIG. 1. (a) Rietveld refinement of XRD data of $NaYbTe_2O_7$. (b) Crystal structure viewed along the a axis. (c) Projection of the one-dimensional Yb chains along the b axis. (d) Possible exchange pathways between nearest magnetic ions.

II. EXPERIMENT

A polycrystalline sample of $NaYbTe_2O_7$ has been prepared by using Na_2CO_3, Yb_2O_3, and TeO_2 as starting materials. Before mixing the starting materials in a stochiometric mixture, Na_2CO_3 was preheated to 373 K to remove the moisture, and Yb_2O_3 was preheated to 1173 K before weighing. The mixture was initially heated to 873 K at a constant ramping rate of 5 K/min to avoid sodium loss through evaporation and kept at the same temperature for 12 hrs. Finally, the mixture was pelletized and heated to 993 K for a pure phase. The synthesized sample has been characterized further on a PANalytical Empyrean Alpha I diffractometer using Cu-Kα single wavelength ($\lambda = 1.54059$ Å). The magnetic properties of the compound have been explored using a magnetic properties measurement system (MPMS) of Quantum Design, USA. Further, magnetization was measured down to 0.4 K using a 3He (iHelium3, Quantum Design Japan) attachment to the MPMS. The physical properties measurement system (PPMS) of Quantum Design, USA, has been utilized to perform heat capacity, ac magnetic susceptibility, and thermal conductivity measurements. For thermal conductivity measurements, the sample was cut into a rectangular shape of the dimensions $1.3 \times 2.9 \times 6.3$ mm^3 and a four probe measurement technique is used. The elemental mapping was performed using the ZEISS Gemini Scanning electron microscope (SEM). Ultralow temperature heat capacity was measured in an Oxford Kelvinox-400MX dilution refrigerator with relaxation calorimetry. A 9.07 mg of the platelike polycrystalline sample was loaded on the sample platform with Apizon-N grease to increase the thermal conductance between the sample and the platform. The two-tau model was used to analyze the data.

III. RESULTS AND DISCUSSION

A. Crystal structure

The atomic arrangement in the unit cell has been determined through Rietveld refinement of the XRD pattern using Jana software [23], and the refined pattern is shown in Fig. 1(a). The close match between the experimental data and the simulated pattern confirmed the phase purity and established that this compound crystallizes in the $P2_1/n$ space group, which is isostructural with $NaYTe_2O_7$, having tellurium in two different oxidation states, (Te^{4+}, Te^{6+}) [24]. The crystal structure obtained from the Rietveld refinement is shown in Fig. 1(b), and the structural parameters are given in Table S1 [25]. In this structure, $Te^{6+}O_6$ octahedra and $Te^{4+}O_4$ dispheniods form a two-dimensional layer of $[Te_2O_7]^{4-}$ stacked along the [1 0 1] direction. A close crystal structure analysis reveals that the YbO_7 polyhedra share an edge through O5 and O7 to form a one-dimensional chain along the b axis, as exhibited in Fig. 1(c). Moreover, energy dispersive spectroscopy analysis reaffirmed the chemical composition of the sample as exhibited in Figs. S1, S2, and Table S2 of the Supplemental Material [25]. The intrachain distance between Yb^{3+} ions is 3.762 Å compared to the interchain distance of 6.271 Å, indicating that the magnetic properties are dominated by intrachain exchange interactions. There are two possible pathways for superexchange interaction, one through O_5 and the other through O_7, featuring different bond angles (Yb-O5-Yb = 113.0°, Yb-O7-Yb = 107.0°) which change their position alternatively similar to $LiCuSbO_4$ [5], as shown in Fig. 1(d). The value of exchange parameters through these paths should be sensitive to bond angle values, as reported for similar magnetic lattices [5], where a subtle change of two degrees can influence the exchange parameters significantly, as reported earlier [26]. Further, frustration is enhanced by the anisotropic nature of the exchange interactions and may lead to a QSL state [27]. Given these compelling structural properties, further exploration of its magnetic ground state holds significant promise.

B. DC magnetization

To investigate the magnetic behavior of this compound, the dc magnetic susceptibility has been measured from 300 to 0.4 K by following the zero-field-cooled (ZFC) and field-cooled (FC) protocols, and the results are depicted in Fig. 2(a) and its inset. It is evident from this figure that there is no long-range magnetic ordering down to 0.4 K. After removing the Van Vleck contribution ($\chi_{VV} = 6.47 \times 10^{-3}$ emu/mol-Oe, estimated from the slope of the linear fitting of isotherms at higher magnetic fields) from the inverse susceptibility data, two different linear regions have been observed, as shown in Fig. S3(a) of the Supplemental Material [25]. Analysis of the inverse susceptibility in the high-temperature (HT) region (125–300 K) gave $\theta_{CW} = -59.81$ K and an effective paramagnetic moment (μ_{eff}) value of 4.65 μ_B/f.u., which is in close

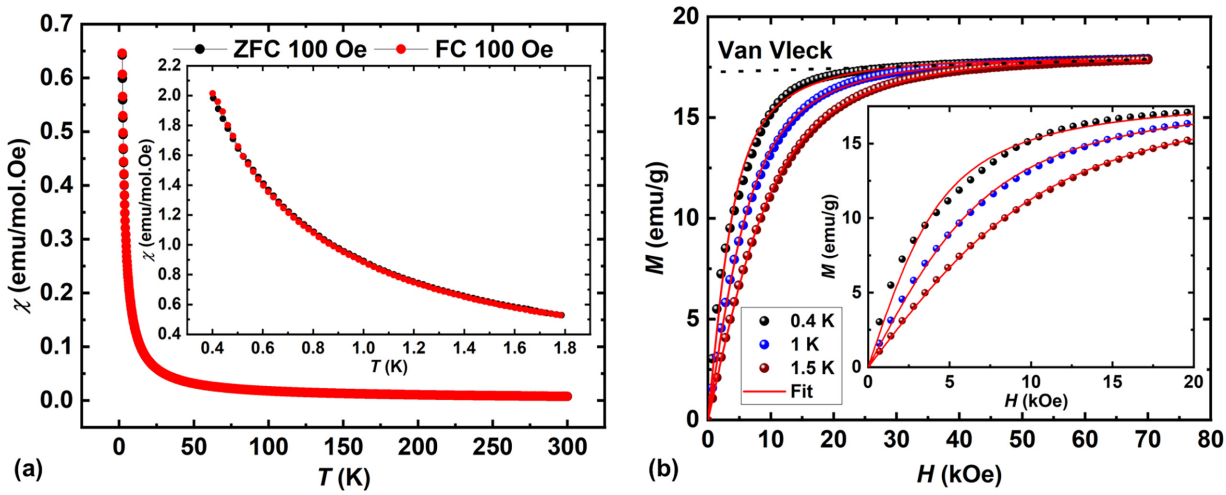

FIG. 2. (a) Temperature dependence of dc magnetic susceptibility performed under ZFC and FC protocol down to 2 K. Inset shows the variation down to 0.4 K. (b) Isothermal magnetization curves measured at different temperatures along with the Brillouin fits represented by solid lines. The black dashed line accounts for the Van Vleck contribution. Inset shows the zoomed version of the fitting in the low-field region.

agreement with the theoretically expected value for Yb^{3+} ions ($J = 7/2, 4f^{13}$ configuration). The Curie constant can be used to calculate the Lande factor (g) as $C = \frac{ng^2\mu_B^2 J(J+1)}{3k_B}$, where n represents the number of free spins per formula unit, μ_B is Bohr magneton, and k_B is Boltzmann constant by assuming that there is no interaction among Yb^{3+} ions at room temperature. The value of g comes out to be 1.17, which is very close to the theoretically expected value, 1.14. The fitting of the low-temperature region (2–50 K) results in a reduced value of $\mu_{\text{eff}} \sim 3.58\ \mu_B$/f.u and $\theta_{CW} = -1.49$ K. Reduction of J value also results in the suppression of the θ_{CW} values. A qualitative alignment between the observed and effective magnetic moments of Yb^{3+} ions at room temperature coupled with the reduced value of the magnetic moment as the temperature is lowered indicates that Yb^{3+} ions have Kramers doublet as the ground state [28–30]. The crystal electric field affects the eightfold degenerate states (for $J = 7/2$) of Yb^{3+} ions and splits them into four Kramers doublet, as observed for other Yb compounds [19–21]. For the LT region ($J_{\text{eff}} = 1/2$), the value of g comes out to be 4.12, which is very close to the g value calculated from isothermal magnetization data (~ 4). The Curie constant is no longer temperature dependent as the higher Kramers doublets also contribute, and considering the temperature range of measurement, it is sufficient to consider only the first excited Kramers doublet. A two-level approximation of the Curie-Weiss model can be expressed as [31,32]

$$1/\chi = 8.(T - \theta_{CW}).\left(\frac{1 + \exp^{-\frac{E_{10}}{k_B T}}}{\mu^2_{\text{eff},0} + \mu^2_{\text{eff},1}.\exp^{-\frac{E_{10}}{k_B T}}}\right), \quad (1)$$

where $\mu^2_{\text{eff},0}$ and $\mu^2_{\text{eff},1}$ stand for effective moments in the crystal field ground state and first excited state while E_{10} denotes the energy separation between the ground and first excited states. Figure S3(b) of the Supplemental Material [25] represents the fitting of the inverse susceptibility data and gives $E_{10} \sim 267$ K, which further confirms the Kramers doublet ground state at lower temperatures.

To examine the high-field magnetism of the compound at low temperatures, we have carried out the isothermal magnetization measurements at three different temperatures, 0.4, 1, and 1.5 K, by gradually varying the magnetic field from +7 T to −7 T. Figure 2(b) depicts the variation of isothermal magnetization curves in the first quadrant. The magnetic isotherm within the paramagnetic state of a compound can be described by $M(H) = \chi_{vv}H + gJ_{\text{eff}}N_A\mu_B B_{J_{\text{eff}}}(H)$, where $B_{J_{\text{eff}}}(H)$ is the Brillouin function [33]. The deviation of magnetization data from the fit below 1 K suggests the development of magnetic correlations [34–36]. The slope of the high-field linear behavior of the magnetization curve at 0.4 K gives the Van Vleck contribution. After subtracting the Van Vleck contribution, the magnetization curve becomes saturated above 2 T. Furthermore, temperature-dependent ac susceptibility measurements have been carried out at the different frequencies of a small ac magnetic field ($H_{ac} = 10$ Oe) to rule out possible glassiness. Figure S4 of the Supplemental Material [25] demonstrates the absence of a glassy state down to 2 K. Hence, a preliminary magnetic investigation reveals the development of magnetic correlations below 1 K.

C. Heat capacity

Heat capacity measurement carried out from 100 to 0.285 K in the absence of a magnetic field is shown in Figs. 3(a) and 3(b), and fitting of the data with the Debye-Einstein model is shown by the solid line. Please note that the compound is highly insulating in the measured temperature range. To access the change in magnetic entropy, removing the lattice contribution from the total heat capacity becomes necessary, which can be estimated using the Debye-Einstein model. This model considers that the sum of acoustic and phonon modes equals the total number of atoms present in the primitive cell (for $NaYbTe_2O_7$, it is 11). Further, the relative weights of acoustical and optical modes are taken in the ratio of 1:n-1, where n is the total number of atoms. So, this compound has three acoustic modes and 30 optical phonon modes. The three acoustic modes have been described using

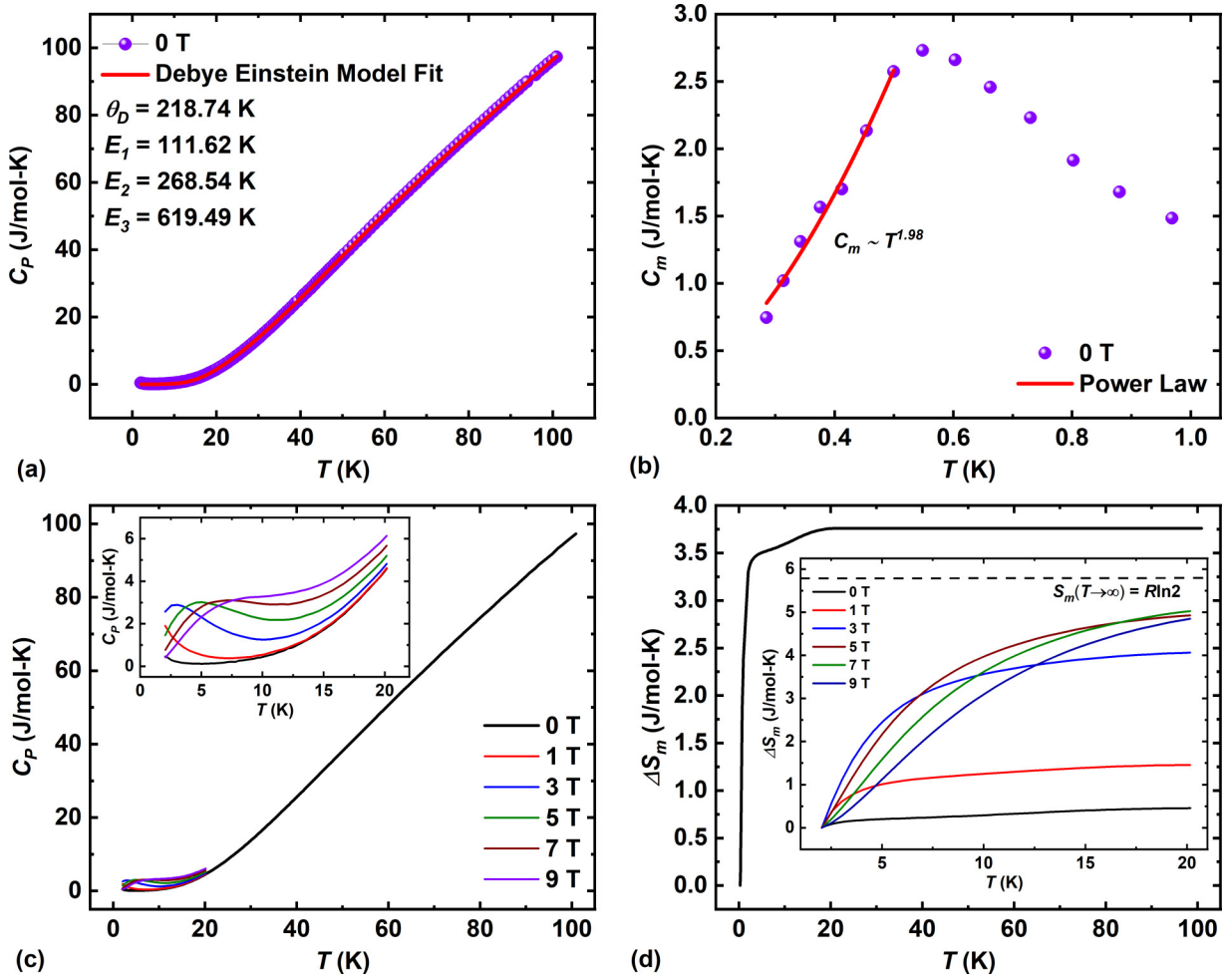

FIG. 3. (a) Fitting of the heat capacity data measured in the absence of the magnetic field with the Debye-Einstein model. (b) Temperature dependence of heat capacity below 1 K and fitting with power law. (c) Temperature dependence of heat capacity data measured under different magnetic fields. The inset shows the variation in low-temperature regions. (d) Entropy calculated from magnetic heat capacity down to 0.285 K. Inset shows the temperature dependence of magnetic entropy calculated down to 2 K in the presence of different magnetic fields.

one Debye term, and three Einstein terms have been used to describe the optical modes. To reduce the free parameters and minimize the experimental errors, several optical modes are grouped [37]. The Debye-Einstein model for this system can be expressed as follows [38,39]:

$$C_{D-E} = \frac{9aR}{x_D^3}\int_0^{x_D}\frac{x^4e^x}{(e^x-1)^2}\,dx + 3R\sum_{i=1}^{3}\frac{b_i x_{E_i}^2 e^{x_{E_i}}}{(e^{x_{E_i}}-1)^2},$$

where $x_{D,E} = \theta_{D,E}/T$, θ_D and θ_E are Debye and Einstein temperatures, respectively, and R is the universal gas constant. The coefficients a and b_i stand for the contributions from acoustic and optical phonons, respectively. The values of these weight factors are constrained in such a way that they add up to the total number of atoms in the unit cell (In this case, $a = 1$, $b_1 = 1$, $b_2 = 3$, and $b_3 = 6$). Here, b_1 corresponds to Te vibrations, b_2 stands for Na^+ and O^{2-} motion, and b_3 represents the contribution from remaining 6 O^{2-} atoms. We could confine the flexible Debye-Einstein model to a physically reasonable fit using these considerations.

The absence of a λ-like anomaly confirms that there is no long-range magnetic ordering down to 0.285 K. However, a broad peak around 0.55 K may be related to magnetic excitations or a weak splitting of degenerate Kramers doublet, which may arise due to local strain on the Yb site [40]. The magnetic contribution below 0.55 K could be fitted well with a power law ($C_m \sim T^n$) with $n \sim 2$, as shown in Fig. 3(b). A similar power law dependence has been observed for other Yb compounds and indicates the presence of a gapless ground state [20,41,42]. A gapped spectral function [$C_m \sim \exp(-\Delta/T)$] could not fit the data, indicating that the broad anomaly is likely due to magnetic excitations. Figure 3(c) depicts that this anomaly moves toward higher temperatures with an increase in the magnetic field, which manifests the Schottky anomaly and rules out possible short-range magnetic ordering. The Schottky anomaly appears due to the splitting of ground state Kramers doublet in an applied magnetic field (Zeeman splitting), as observed for other Yb compounds [35,43]. The magnetic entropy has been estimated by subtracting the phononic contribution, and its temperature dependence is shown in Fig. 3(d). A comparison of the calculated magnetic entropy with the theoretically expected value for $J_{\text{eff}} = 1/2$ unveils that ~35% of the magnetic entropy is still embedded into the system below 0.285 K. The saturation value of the

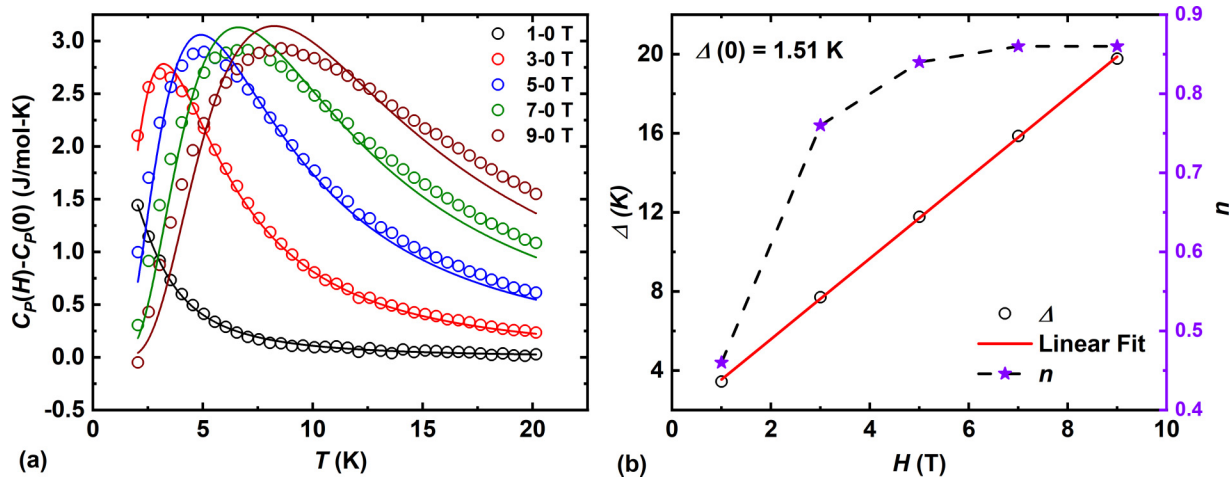

FIG. 4. (a) Variation of Schottky contribution with temperature and its fitting with the two-level model equation. (b) Linear fitting of Δ (left axis) values calculated from the CEF fitting and variation of n values with the magnetic fields

magnetic entropy increases with an increase in magnetic field and approaches around $Rln2$ above 5 T, as shown in the inset of Fig. 3(d). A slightly lower saturation value of the magnetic entropy than $Rln2$ indicates that a smaller fraction of the spins are randomly oriented.

In the presence of a magnetic field, total heat capacity can be written as $C(T,H) = C(T,0) + C_{sch}(T,H)$. Hence, the Schottky contribution can be probed by subtracting the zero field heat capacity from the total heat capacity measured under finite magnetic fields. Considering $J_{\text{eff}} = 1/2$ (two-level system), Schottky anomaly can be expressed as [44–46]

$$C_{sch}(T,H) = nR\left(\frac{\Delta}{T^2}\right)\frac{\exp(\Delta/T)}{[1+\exp(\Delta/T)]^2}, \qquad (2)$$

where n represents the number of free spins per formula unit, R is the universal gas constant, and Δ determines the spacing between two levels. Δ has a magnetic field dependence which can be expressed as [45–48] $\Delta(H) = g\mu_B H_{\text{eff}}/k_B$, where $H_{\text{eff}} = \sqrt{H_0^2 + H_1^2}$ which implies that $H_{\text{eff}} = H_0$ in the absence of the external magnetic field ($H_1 = 0$). Figure 4(a) exhibits the fitting of Schottky contribution data at different magnetic fields. We observed that the Schottky contribution for $H > 5$ T could not be fitted well with a two-level model, and the inclusion of the third or fourth level is required. The variation of the fitted parameters with the magnetic field is shown in Fig. 4(b). The intercept of the linear fit of crystal field energy gives its value at zero field, $\Delta(0) \sim 1.51$ K. A finite value of $\Delta(0)$ originates from the development of Yb^{3+}-Yb^{3+} correlations [35,36,43]. In the case of n, it first increases up to 5 T and then exhibits a saturation behavior, suggesting that the energy levels are split by the magnetic field and around 86% of the spins are excited to higher energy levels. The fraction of spins excited to higher levels in the presence of a magnetic field matches exactly with the amount of the magnetic entropy recovered (∼86%), as depicted in Fig. 3(d). The value of Lande g factor comes out to be ∼3.27 considering the relation $\Delta(H) = g\mu_B H_{\text{eff}}/k_B$ [taking $\Delta(H) =$ 19.78 K for $H = 9$ T].

D. Thermal conductivity

Considering the presence of Schottky anomaly in the heat capacity measurements, measuring thermal conductivity will be more helpful as it does not respond to localized entities responsible for Schottky anomaly but is only sensitive to the itinerant excitations [49]. Heat is transported mainly by acoustic phonons and magnetic contributions for low-dimensional magnetic systems [50,51]. Figure 5(a) exhibits a broad feature in κ/T data centered around 20 K where phonon contribution dominates the thermal conductivity. This feature has been observed for many systems [52,53] and can be explained by the Callaway model of thermal conductivity [54], according to which a decrease in phonon population with a decrease in the temperature and an increase in phonon mean free path in a finite-sized sample can result in such a feature. Figure 5(b) shows the fitting of the zero field κ/T data with $\kappa/T = a + bT^{\alpha-1}$, where the first term represents electronlike contribution (for insulators, it should be zero) and the second term is responsible for the phononic contribution. The fitting results in T^3 dependence of the thermal conductivity, which confirms the diffuse scattering of the phonons and rules out the presence of the specular scattering. Further, a finite value of a under 0 T and its magnetic field dependence (as shown in Table I) indicates the presence of magnetic excitations in the system. Moreover, the value of α decreases with an increase in the magnetic field (all the fittings shown in Fig. S5 of the Supplemental Material [25]), manifesting that the spins are getting ordered and contributing toward thermal resistance

TABLE I. Magnetic field dependence of a and α parameter.

H (T)	a (W/ K^2-m)	α
0	0.00958	3.0843
1	0.01052	3.1788
3	0.01167	2.6685
5	0.00898	2.7696
7	0.00748	2.4631
9	0.00786	2.5823

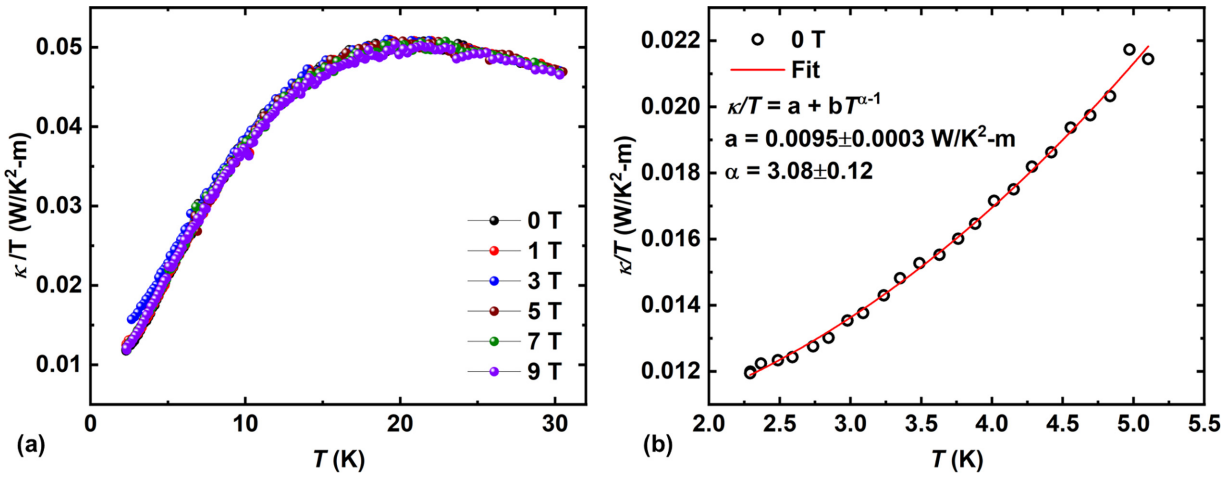

FIG. 5. (a) Temperature dependence of the thermal conductivity divided by temperature measured under different magnetic fields. (b) Fitting of κ/T measured under 0 T with the equation described in the text.

(although very small). The magnetic field dependence of α is consistent with the magnetic entropy values, further supporting our claim of magnetic excitations.

IV. CONCLUSION

In conclusion, we have undertaken a comprehensive characterization of a quasi-one-dimensional magnet, $NaYbTe_2O_7$, employing various magnetic and thermodynamic measurement techniques. This unique material features well-separated, one-dimensional zig-zag magnetic chains of Yb^{3+} ions along the b axis, presenting an ideal platform for investigating one-dimensional magnetic properties. Our DC magnetization measurements have notably demonstrated the absence of long-range magnetic ordering down to temperatures as low as 0.4 K, despite antiferromagnetic interactions suggested by a higher θ_{CW} value. Analyzing the low-temperature region of the inverse susceptibility has allowed us to identify the ground state as the Kramers doublet with $J = 1/2$, signifying the strong spin correlation evident in the slight deviation of low-temperature magnetic isotherms from the Brillouin function. Furthermore, our heat capacity measurements exhibited no lambda-like anomaly down to 0.285 K, and the magnetic field dependence of these measurements has revealed a discernible crystal electric field, reinforcing the Yb^{3+}-Yb^{3+} correlations. The presence of the Schottky anomaly further confirms the Zeeman splitting, while thermal conductivity measurements have unveiled the existence of magnetic excitations in the system. Considering these collective findings, and the anisotropic and bond-sensitive nature of the exchange interactions between Yb^{3+} ions, $NaYbTe_2O_7$ holds promise as a potential candidate for a gapless quantum spin liquid. To delve deeper into its properties, sub-Kelvin investigations using local probes, such as μSR and inelastic neutron scattering, are warranted.

ACKNOWLEDGMENTS

The authors thank Mr. Sudip Ghosh for his help in various measurements. The authors are thankful to the School of Advanced Materials, Jawaharlal Nehru Centre for Advanced Scientific Research (JNCASR), for providing a number of experimental facilities. The authors also thank the International Centre for Materials Science (ICMS) and Sheikh Saqr Laboratory (SSL). A.S. is thankful to the Department of Science & Technology (DST) for Grant No. DST/NM/TUE/QM-10/2019 (G)/3. R.K. is thankful to the Council of Scientific and Industrial Research (CSIR) for the Ph.D. fellowship [Grant No. 09/733(0263/2019-EMR-I)]. Work at SNU was supported by the BrainLink program through the NRF of Korea (2022H1D3A3A01077468 and RS-2024-00338707).

[1] U. Schollwöck, J. Richter, D. J. J. Farnell, and R. F. Bishop, *Qauntum Magnetism* (Springer, Berlin Heidelberg, 2008).

[2] S.-L. Drechsler, J. Richter, A. A. Gippius, A. Vasiliev, A. A. Bush, A. S. Moskvin, J. Málek, Y. Prots, W. Schnelle, and H. Rosner, Helical ground state and weak ferromagnetism in the edge-shared chain cuprate $NaCu_2O_2$, Europhys. Lett. **73**, 83 (2006).

[3] M. Härtel, J. Richter, D. Ihle, and S.-L. Drechsler, Thermodynamics of a one-dimensional frustrated spin-1/2 Heisenberg ferromagnet, Phys. Rev. B **78**, 174412 (2008).

[4] H. T. Lu, Y. J. Wang, S. Qin, and T. Xiang, Zigzag spin chains with antiferromagnetic-ferromagnetic interactions: Transfer-matrix renormalization group study, Phys. Rev. B **74**, 134425 (2006).

[5] S. E. Dutton, M. Kumar, M. Mourigal, Z. G. Soos, J.-J. Wen, C. L. Broholm, N. H. Andersen, Q. Huang, M. Zbiri, R. Toft-Petersen, and R. J. Cava, Quantum spin liquid in frustrated one-dimensional $LiCuSbO_4$, Phys. Rev. Lett. **108**, 187206 (2012).

[6] W. E. A. Lorenz, R. O. Kuzian, S.-L. Drechsler, W.-D. Stein, N. Wizent, G. Behr, J. Malek, U. Nitzsche, H. Rosner, A. Hiess

et al., Highly dispersive spin excitations in the chain cuprate Li_2CuO_2, Europhys. Lett. **88**, 37002 (2009).

[7] S. Park, Y. J. Choi, C. L. Zhang, and S-W. Cheong, Ferroelectricity in an $S = 1/2$ chain cuprate, Phys. Rev. Lett. **98**, 057601 (2007).

[8] S. Seki, Y. Yamasaki, M. Soda, M. Matsuura, K. Hirota, and Y. Tokura, Correlation between spin helicity and an electric polarization vector in quantum-spin chain magnet $LiCu_2O_2$, Phys. Rev. Lett. **100**, 127201 (2008).

[9] M. Matsuda and K. Katsumata, Magnetic properties of a quasi-one-dimensional magnet with competing interactions: $SrCuO_2$, J. Magn. Magn. Mater. **140-144**, 1671 (1995).

[10] M. Enderle, C. Mukherjee, B. Fak, R. K. Kremer, J.-M. Broto, H. Rosner, S.-L. Drechsler, J. Richter, J. Malek, A. Prokofiev *et al.*, Quantum helimagnetism of the frustrated spin-$\frac{1}{2}$ chain $LiCuVO_4$, Europhys. Lett. **70**, 237 (2005).

[11] M. Mourigal, M. Enderle, R. K. Kremer, J. M. Law, and B. Fak, Ferroelectricity from spin supercurrents in $LiCuVO_4$, Phys. Rev. B **83**, 100409(R) (2011).

[12] M. Enderle, B. Fak, H.-J. Mikeska, R. K. Kremer, A. Prokofiev, and W. Assmus, Two-spinon and four-spinon continuum in a frustrated ferromagnetic spin-1/2 chain, Phys. Rev. Lett. **104**, 237207 (2010).

[13] S.-L. Drechsler, O. Volkova, A. N. Vasiliev, N. Tristan, J. Richter, M. Schmitt, H. Rosner, J. Malek, R. Klingeler, A. A. Zvyagin *et al.*, Frustrated cuprate route from antiferromagnetic to ferromagnetic spin-1/2 heisenberg chains: Li_2ZrCuO_4 as a missing link near the quantum critical point, Phys. Rev. Lett. **98**, 077202 (2007).

[14] M. Hase, H. Kuroe, K. Ozawa, O. Suzuki, H. Kitazawa, G. Kido, and T. Sekine, Magnetic properties of $Rb_2Cu_2Mo_3O_{12}$ including a one-dimensional spin-1/2 Heisenberg system with ferromagnetic first-nearest-neighbor and antiferromagnetic second-nearest-neighbor exchange interactions, Phys. Rev. B **70**, 104426 (2004).

[15] M. Hase, K. Ozawa, O. Suzuki, H. Kitazawa, G. Kido, H. Kuroe, and T. Sekine, Magnetism of $A_2Cu_2Mo_3O_{12}$ (A = Rb or Cs): Model compounds of a one-dimensional spin-1/2 Heisenberg system with ferromagnetic first-nearest-neighbor and antiferromagnetic second-nearest-neighbor interactions, J. Appl. Phys. **97**, 10B303 (2005).

[16] L. S. Wu, S. E. Nikitin, Z. Wang, W. Zhu, C. D. Batista, A. M. Tsvelik, A. M. Samarakoon, D. A. Tennant, M. Brando, L. Vasylechkov *et al.*, Tomonaga-Luttinger liquid behavior and spinon confinement in $YbAlO_3$, Nat. Commun. **10**, 698 (2019).

[17] N. Zhao, J. Sheng, J. Wang, H. Ge, T. Li, J. Yang, S. Wang, P. Miao, H. He, X. Tong *et al.*, Quasi-one-dimensional Ising-like antiferromagnetism in the rare-earth perovskite oxide $TbScO_3$, Phys. Rev. Mater. **7**, 034401 (2023).

[18] L. S. Wu, W. J. Gannon, I. A. Zaliznyak, A. M. Tsvelik, M. Brockmann, J.-S. Caux, M. S. Kim, Y. Qiu, J. R. D. Copley, G. Ehlers *et al.*, Orbital-exchange and fractional quantum number excitations in an f-electron metal, Yb_2Pt_2Pb, Science **352**, 1206 (2016).

[19] Y. Li, D. Adroja, R. I. Bewley, D. Voneshen, A. A. Tsirlin, P. Gegenwart, and Q. Zhang, Crystalline electric-field randomness in the triangular lattice spin-liquid $YbMgGaO_4$, Phys. Rev. Lett. **118**, 107202 (2017).

[20] L. Ding, P. Manuel, S. Bachus, F. Grußler, P. Gegenwart, J. Singleton, R. D. Johnson, H. C. Walker, D. T. Adroja, A. D. Hillier *et al.*, Gapless spin-liquid state in the structurally disorder-free triangular antiferromagnet $NaYbO_2$, Phys. Rev. B **100**, 144432 (2019).

[21] J. G. Rau, L. S. Wu, A. F. May, L. Poudel, B. Winn, V. O. Garlea, VO, A. Huq, P. Whitfield, A. E. Taylor, M. D. Lumsden *et al.*, Anisotropic exchange within decoupled tetrahedra in the quantum breathing pyrochlore $Ba_3Yb_2Zn_5O_{11}$, Phys. Rev. Lett. **116**, 257204 (2016).

[22] J. A. M. Paddison, M. Daum, Z. Dun, G. Ehlers, Y. Liu, M. B. Stone, H. Zhou, and M. Mourigal, Continuous excitations of the triangular-lattice quantum spin liquid $YbMgGaO_4$, Nat. Phys. **13**, 117 (2017).

[23] V. Petříček, M. Dušek, and L. Palatinus, Crystallographic computing system JANA2006: General features, Z. Kristallogr. Cryst. Mater. **229**, 345 (2014).

[24] H. Xia, J. Shen, Z. Zhu, Y. Lv, Q. Ma, and H. Wang, $NaYTe_2O_7$: A new compound with mixed valence of tellurium and large birefringence, J. Alloys Compd. **816**, 152535 (2020).

[25] See Supplemental Material at http://link.aps.org/supplemental/10.1103/PhysRevB.109.224429 for crystallographic parameters, energy dispersive spectroscopy results, analysis of the inverse susceptibility data, and fitting of magnetic field dependent κ/T data.

[26] J. G. Rau and M. J. P. Gingras, Frustration and anisotropic exchange in ytterbium magnets with edge-shared octahedra, Phys. Rev. B **98**, 054408 (2018).

[27] Y. Li, G. Chen, W. Tong, L. Pi, J. Liu, Z. Yang, X. Wang, and Q. Zhang, Rare-earth triangular lattice spin liquid: A single-crystal study of $YbMgGaO_4$, Phys. Rev. Lett. **115**, 167203 (2015).

[28] H. W. J. Blöte, R. F. Wielinga, and W. J. Huiskamp, Heat-capacity measurements on rare-earth double oxides $R_2M_2O_7$, Physica **43**, 549 (1969).

[29] H. B. Cao, A. Gukasov, I. Mirebeau, and P. Bonville, Anisotropic exchange in frustrated pyrochlore $Yb_2Ti_2O_7$, J. Phys.: Condens. Matter **21**, 492202 (2009).

[30] S. Guo, A. Ghasemi, C. L. Broholm, and R. J. Cava, Magnetism on ideal triangular lattices in $NaBaYb(BO_3)_2$, Phys. Rev. Mater. **3**, 094404 (2019).

[31] T. Besara, M. S. Lundberg, J. Sun, D. Ramirez, L. Dong, J. B. Whalen, R. Vasquez, F. Herrera, J. R. Allen, M. W. Davidson *et al.*, Single crystal synthesis and magnetism of the $BaLn_2O_4$ family (Ln = lanthanide), Prog. Solid State Chem. **42**, 23 (2014).

[32] M. Mitric, B. Antic, M. Balanda, D. Rodic, and M. L. Napijalo, An x-ray diffraction and magnetic susceptibility study of $Yb_xY_{2-x}O_3$, J. Phys.: Condens. Matter **9**, 4103 (1997).

[33] C. Kittel, *Introduction to Solid State Physics* (Wiley, Hoboken, NJ, 2005).

[34] R. Sibille, E. Lhotel, V. Pomjakushin, C. Baines, T. Fennell, and M. Kenzelmann, Candidate quantum spin liquid in the Ce^{3+} pyrochlore stannate $Ce_2Sn_2O_7$, Phys. Rev. Lett. **115**, 097202 (2015).

[35] K. Somesh, S. S. Islam, S. Mohanty, G. Simutis, Z. Guguchia, C. Wang, J. Sichelschmidt, M. Baenitz, R. Nath, Absence of magnetic order and emergence of unconventional fluctuations in the $J_{\text{eff}} = 1/2$ triangular-lattice antiferromagnet $YbBO_3$, Phys. Rev. B **107**, 064421 (2023).

[36] S. Kundu, A. Hossain, Pranava Keerthi S, R. Das, M. Baenitz, P. J. Baker, J.-C. Orain, D. C. Joshi, R. Mathieu, P. Mahadevan,

S. Pujari, S. Bhattacharjee, A. V. Mahajan, and D. D. Sarma, Signatures of a spin-1/2 cooperative paramagnet in the diluted triangular lattice of Y_2CuTiO_6, Phys. Rev. Lett. **125**, 117206 (2020).

[37] P. Svoboda, J. Vejpravova, N.-T. Kim-Ngan, and F. Kaysel, Specific heat study of selected RNi_5, J. Magn. Magn. Mater. **272-276**, 595 (2004).

[38] R. Kumar and A. Sundaresan, Unveiling a hidden multiferroic state under magnetic fields in $BaHoFeO_4$, Phys. Rev. B **107**, 184420 (2023).

[39] R. Kumar and A. Sundaresan, Antisite disorder driven cluster glass state and colossal magnetoresistance in $MnSb_2Se_4$, Phys. Rev. B **106**, 134423 (2022).

[40] J. van Duijn, K. H. Kim, N. Hur, D. Adroja, M. A. Adams, Q. Z. Huang, M. Jaime, S.-W. Cheong, C. Broholm, and T. G. Perring, Inhomogeneous level splitting in $Pr_{2-x}Bi_xRu_2O_7$, Phys. Rev. Lett. **94**, 177201 (2005).

[41] Y. Li, H. Liao, Z. Zhang, S. Li, F. Jin, L. Ling, L. Zhang, Y. Zou, L. Pi, Z. Yang, J. Wang, Z. Wu, and Q. Zhang, Gapless quantum spin liquid ground state in the two-dimensional spin-1/2 triangular antiferromagnet $YbMgGaO_4$, Sci. Rep. **5**, 16419 (2015).

[42] Z. Ma, J. Wang, Z.-Y. Dong, J. Zhang, S. Li, S.-H. Zheng, Y. Yu, W. Wang, L. Che, K. Ran, S. Bao, Z. Cai, P. Cermak, A. Schneidewind, S. Yano, J. S. Gardner, X. Lu, S.-L. Yu, J.-M. Liu, S. Li *et al.* Spin-glass ground state in a triangular-lattice compound $YbZnGaO_4$, Phys. Rev. Lett. **120**, 087201 (2018).

[43] R. Bag, M. Ennis, C. Liu, S. E. Dissanayake, Z. Shi, J. Liu, L. Balents, and S. Haravifard, Realization of quantum dipoles in triangular lattice crystal $Ba3Yb(BO_3)_3$, Phys. Rev. B **104**, L220403 (2021).

[44] H. M. Rosenberg, *Low Temperature Solid State Physics* (Oxford University Press, Oxford, 1963).

[45] L. Xie, T. Su, and X. Li, Magnetic field dependence of Schottky anomaly in the specific heats of stripe-ordered superconductors $La_{1.6-x}Nd_{0.4}Sr_xCuO_4$, Physica C: Superconductivity **480**, 14 (2012).

[46] S. Mahdavifar and A. Akbari, Heat capacity of Schottky type in low-dimensional spin systems, J. Phys.: Condens. Matter **20**, 215213 (2008).

[47] G. Mu, Y. Wang, L. Shan, and H.-H. Wen, Possible nodeless superconductivity in the noncentrosymmetric superconductor $Mg_{12-\delta}Ir_{19}B_{16}$, Phys. Rev. B **76**, 064527 (2007).

[48] Y. Wang, J. Yan, L. Shan, H.-H. Wen, Y. Tanabe, T. Adachi, and Y. Koike, Weak-Coupling d-wave BCS superconductivity and unpaired electrons in overdoped $La_{2-x}Sr_xCuO_4$ single crystals, Phys. Rev. B **76**, 064512 (2007).

[49] M. Yamashita, N. Nakata, Y. Kasahara, T. Sasaki, N. Yoneyama, N. Kobayashi, S. Fujimoto, T. Shibauchi, and Y. Matsuda, Thermal-transport measurements in a quantum spin-liquid state of the frustrated triangular magnet κ-$(BEDT\text{-}TTF)_2Cu_2(CN)_3$, Nat. Phys. **5**, 44 (2009).

[50] B. C. Sales, M. D. Lumsden, S. E. Nagler, D. Mandrus, and R. Jin, Magnetic field enhancement of heat transport in the 2d heisenberg antiferromagnet $K_2V_3O_8$, Phys. Rev. Lett. **88**, 095901 (2002).

[51] S. Y. Li, L. Taillefer, C. H. Wang, and X. H. Chen, Ballistic magnon transport and phonon scattering in the antiferromagnet Nd_2CuO_4, Phys. Rev. Lett. **95**, 156603 (2005).

[52] M. Yamashita, N. Nakata, Y. Senshu, M. Nagata, H. M. Yamamoto, R. Kato, T. Shibauchi, and Y. Matsuda, Highly mobile gapless excitations in a two-dimensional candidate quantum spin liquid, Science **328**, 1246 (2010).

[53] P. Bourgeois-Hope, F. Laliberte, E. Lefrançois, G. Grissonnanche, S. Rene de Cotret, R. Gordon, S. Kitou, H. Sawa, H. Cui, R. Kato, L. Taillefer, and N. Doiron-Leyraud, Thermal conductivity of the quantum spin liquid candidate $EtMe_3Sb[Pb(dmit)_2]_2$, Phys. Rev. X **9**, 041051 (2019).

[54] J. Callaway, Model for lattice thermal conductivity at low temperatures, Phys. Rev. **113**, 1046 (1959).